The mass normalisation of the displacement and strain mode shapes in a strain experimental modal analysis using the mass-change strategy

Tadej Kranjc[1], Janko Slavič[2], Miha Boltežar*[2]

March 21, 2014

Cite as:

Kranjc, T., Slavič, J. and Boltežar, M., **The mass normalisation of the displacement and strain mode shapes in a strain experimental modal analysis using the mass-change strategy**, Journal of Sound and Vibration, Volume 332, Issue 26, 23 December 2013, Pages 6968-6981, ISSN 0022-460X, http://dx.doi.org/10.1016/j.jsv.2013.08.015.

---

[1] Ydria Motors d.o.o., Podskrajnik 16, 1380 Cerknica, Slovenia-EU.
[2] Faculty of Mechanical Engineering, University of Ljubljana, Aškerčeva 6, 1000 Ljubljana, Slovenia-EU.

* Corresponding author: Miha Boltežar, miha.boltezar@fs.uni-lj.si, +386 1 4771 608

Abstract

The classic experimental modal analysis (EMA) is a well-known procedure for determining the modal parameters. The less frequently used strain EMA is based on a response measurement using strain sensors. The results of a strain EMA are the modal parameters, where in addition to the displacement mode shapes the strain mode shapes are also identified. The strain EMA can be used for an experimental investigation of a stress-strain distribution without the need to build a dynamical model. It can also be used to determine the modal parameters when, during modal testing, a motion sensor cannot be used and so a strain sensor is used instead. The displacement and strain mode shapes that are determined with the strain EMA are not mass normalised (scaled with respect to the orthogonality properties of the mass-normalised modal matrix), and therefore some dynamical properties of the system cannot be obtained. The mass normalisation can be made with the classic EMA, which requires the use of a motion sensor. In this research a new approach to the mass normalisation in the strain EMA, without using a motion sensor, is presented.

It is based on the recently introduced mass-change structural modification method, which is used for the mass normalisation in an operational modal analysis. This method was modified in such a way that it can be used for the mass normalisation in the strain EMA. The mass-normalised displacement and strain mode shapes were obtained using a combination of the proposed approach and the strain EMA. The proposed approach was validated on real structures (beam and plate).

1 Introduction

In a modal analysis the displacement mode shapes (eigenvectors) are usually subjected to a scaling procedure, referred to as mass-normalisation, with respect to the orthogonality properties of the mass-normalised modal matrix [1, 2]. When the displacement mode shapes of a dynamical system are not scaled in this manner they cannot be used for the calculation of the mass and stiffness matrices [1, 2, 3]. The mass-normalised displacement mode shapes of a real structure are usually determined with an experimental modal analysis (EMA) [1, 2, 4, 5], which is also used to determine the other modal parameters. The modal parameters can also be determined with the less-frequently used strain EMA [3, 6], where the response is measured with a strain sensor. In addition to the modal parameters, the strain mode shapes can also be determined [3, 6]. However, in the strain EMA the mass normalisation of the displacement and the strain mode shapes cannot be performed [3, 6, 7].

Some of the early researches relating to strain EMA include [3, 6, 8, 9, 10]. Young and Joanides [9] predicted the strains from a modal model that was derived from test data. Hillary and Ewins [8] indirectly determined the external dynamic forces with a strain measurement. Kamrower and Pakstys [10] used the strain values that were obtained from a modal test using accelerometers and strain gauges to predict the strains under the impact loadings. The sound theoretical and practical aspects of the strain EMA were presented by Bernasconi and Ewins [3, 6]. The strain EMA can be used for an experimental investigation of the stress-strain distribution of a real structure without building a mathematical model [11]. The strain EMA should also be applied when a response cannot be measured with a motion sensor and a strain sensor can be used instead (*i.e.*, in a displacement mode shape node with no motion, where the strains are not zero, *e.g.*, the area near the clamped boundary condition). In some circumstances the strain sensor should be used because the motion sensor is inadequate (*e.g.*, in a magnetic flux environment the fiber Bragg grating strain sensor [12] can be used instead of accelerometers that are often sensitive to magnetism [13]). A drawback of the strain EMA is that the displacement and strain mode shapes that are obtained from the strain EMA are not mass normalised [3, 6, 7]. They only have relative information about the mass-normalised displacement and the strain mode shapes. Some researchers proposed a mass normalisation with the classic EMA [3, 6, 11], that requires an additional response measurement with a motion sensor. However, when the measurement of a response with a motion sensor in the strain EMA is not possible, the mass-normalisation procedure cannot be experimentally performed.

Similar problems regarding mass normalisation also occur in the field of Operational Modal Analysis (OMA). The OMA [14] is an output-only modal method, where the excitation is performed with the ambient forces, and therefore only the relative values of the displacement mode shapes are obtained. In the OMA the mass normalisation of the displacement mode shapes can be made with the recently introduced, sensitivity-based, mass-normalisation methods, which are based on the natural frequency shifts due to a structural modification [15]. Sensitivity-based mass normalisation where the structure modification is performed by adding masses was first presented by Parloo *et al.* [15] and later also by others, *e.g.*, [16, 17, 18, 19]. This method is usually referred to as the mass-change strategy. The structure modification can also be performed by the stiffness changes [20]. Khatibi *et al.* [21] found that adding masses has a small effect on the first natural frequency. The effect of a structure modification resulting from the stiffness change is higher; therefore, they proposed the mass-stiffness change strategy, which produces more accurate results than the mass-change strategy, especially for the first mode.

In this research a new approach for the mass-normalisation of the displacement and strain mode shapes in a strain EMA is proposed that eliminates the need for a motion sensor [3, 6, 11]. It is based on the recently introduced mass-change strategy for OMA [15, 16, 18], which was modified in such a way that it was applicable to the strain EMA. The mass-normalised displacement and strain mode shapes were obtained by integrating the modified mass-change strategy and the strain EMA. The effects on the accuracy of the proposed approach have also been researched. The validation of the proposed approach involved experimental tests on a free-free supported beam and plate.

The paper is organized as follows: In Section 2.1 the theory of the strain response of a dynamical system is presented. This is followed by the strain EMA theory in Section 2.2 and the specification of the problems regarding the mass normalisation in Section 2.3. In Section 2.4 and 2.5 the mass-change strategy for the OMA and the modified mass-change strategy for the strain EMA are presented, respectively. The effects on the accuracy of the proposed approach are analyzed in Section 2.6. Section 3 presents the experimental validation of the proposed approach. The conclusion follows in Section 4.

2 Theoretical background

2.1 The strain response of a dynamical system

The strain response of a dynamical system will be derived from the motion response. The motion steady-state response $\mathbf{X}(\omega)$ of the hysteretically proportionally damped dynamical system can be written as [1, 2]:

$$\mathbf{X}(\omega) = \mathbf{\Phi}\ \left[^{\diagdown}\omega_r^2(1+\mathrm{i}\,\eta_r) - \omega^2{}_{\diagdown}\right]^{-1}\ \mathbf{\Phi}^{\mathrm{T}}\,\mathbf{F}(\omega) = \mathbf{H}(\omega)\,\mathbf{F}(\omega), \tag{1}$$

where $\mathbf{\Phi}$ is the modal matrix (matrix of mass-normalised displacement mode shapes), ω_r are the natural frequencies, η_r are the damping loss factors, $\mathbf{F}(\omega)$ is the vector of the excitation force, $\mathbf{H}(\omega)$ is the receptance matrix and $[^{\diagdown}{}_{\diagdown}]$ denotes a diagonal matrix.

To research the system response with respect to the strains the operator $\mathbf{S}$ is introduced [3, 22]:

$$\mathbf{S} = \frac{1}{2}(\nabla + \nabla^{\mathrm{T}}) \tag{2}$$

where ∇ is the linear differential operator in the space domain. $\mathbf{S}$ converts the displacement field to the strain field. When $\mathbf{S}$ is applied to the rth mass-normalised displacement mode shape $\mathbf{\Phi}_r$, the mass-normalised strain mode shape $\mathbf{\Phi}_r^{\varepsilon}$ is obtained [3, 7, 23]:

$$\mathbf{\Phi}_r^{\varepsilon} = \mathbf{S}\mathbf{\Phi}_r \tag{3}$$

where $\mathbf{\Phi}_r^{\varepsilon}$ represents strains corresponding to $\mathbf{\Phi}_r$. Applying the operator $\mathbf{S}$ to Eq. (1) results to the strain steady-state response $\mathbf{X}^{\varepsilon}(\omega)$ [3, 7, 23]:

$$\mathbf{X}^{\varepsilon}(\omega) = \mathbf{\Phi}^{\varepsilon}\ \left[^{\diagdown}\omega_r^2(1+\mathrm{i}\,\eta_r) - \omega^2{}_{\diagdown}\right]^{-1}\ \mathbf{\Phi}^{\mathrm{T}}\,\mathbf{F}(\omega) = \mathbf{H}^{\varepsilon}(\omega)\,\mathbf{F}(\omega) \tag{4}$$

where $\mathbf{H}^{\varepsilon}(\omega)$ is the strain Frequency-Response Function (FRF) matrix and $\mathbf{\Phi}^{\varepsilon}$ is the matrix of mass-normalised strain mode shapes. $\mathbf{H}^{\varepsilon}(\omega)$ can be writen as [11]:

$$\mathbf{H}^{\varepsilon}(\omega) = \sum_{r=1}^{N} \frac{{}_r\mathbf{A}^{\varepsilon}}{\omega_r^2 - \omega^2 + \mathrm{i}\,\eta_r\,\omega_r^2} \tag{5}$$

where ${}_r\mathbf{A}^{\varepsilon}$ is the strain modal constants matrix, corresponding to the rth mode and can be written as:

$${}_r\mathbf{A}^{\varepsilon} = \begin{bmatrix} \phi_{1r}^{\varepsilon}\phi_{1r} & \cdots & \phi_{1r}^{\varepsilon}\phi_{kr} & \cdots & \phi_{1r}^{\varepsilon}\phi_{N_\mathrm{d}r} \\ \vdots & \ddots & \vdots & \ddots & \vdots \\ \phi_{jr}^{\varepsilon}\phi_{1r} & \cdots & \phi_{jr}^{\varepsilon}\phi_{kr} & \cdots & \phi_{jr}^{\varepsilon}\phi_{N_\mathrm{d}r} \\ \vdots & \ddots & \vdots & \ddots & \vdots \\ \phi_{N_\mathrm{s}r}^{\varepsilon}\phi_{1r} & \cdots & \phi_{N_\mathrm{s}r}^{\varepsilon}\phi_{kr} & \cdots & \phi_{N_\mathrm{s}r}^{\varepsilon}\phi_{N_\mathrm{d}r} \end{bmatrix}_{N_\mathrm{s}\times N_\mathrm{d}} \tag{6}$$

where ϕ_{jr}^{ε} and ϕ_{kr} are the components of $\mathbf{\Phi}_r^{\varepsilon}$ and $\mathbf{\Phi}_r$, respectively. N_d and N_s are the sizes of $\mathbf{\Phi}_r$ and $\mathbf{\Phi}_r^{\varepsilon}$, respectively. Eq. (6) shows that ${}_rA_{jk}^{\varepsilon} \neq {}_rA_{kj}^{\varepsilon}$; therefore, $\mathbf{H}^{\varepsilon}$ is not symmetric $(H_{jk}^{\varepsilon} \neq H_{kj}^{\varepsilon})$. $\mathbf{H}^{\varepsilon}$ is generally not a square matrix [11].

2.2 Strain EMA

The strain EMA can be used for determining the dynamical properties of a real structure, similar to the classic EMA [3, 6]. During the strain modal testing a structure is excited with a known force at the structure point k and the response is determined with a strain measurement at the point j. From the time input-output signals the strain FRF H^{ε}_{jk} is obtained using the same FRF estimators [2] as in the classic EMA. When the information about the displacement and the strain mode shapes need to be obtained at least one row and one column of the strain FRF matrix need to be experimentally determined [11].

The identification of the natural frequencies and the damping is performed in a similar way as in the classic EMA [11]. The results of an indirect (modal) identification method [2] are the natural frequencies, the damping [24], the strain modal constants and their phases for all the measured strain FRF. The strain modal constants that are identified from the jth row and the kth column of the strain FRF matrix are denoted as ${}_r\mathbf{A}^{\varepsilon}_j = \phi^{\varepsilon}_{jr}\,\boldsymbol{\Phi_r}$ and ${}_r\mathbf{A}^{\varepsilon}_k = \boldsymbol{\Phi}^{\varepsilon}_r\,\phi_{kr}$, respectively (see Eq. (5) and (6)). ${}_r\mathbf{A}^{\varepsilon}_j$ and ${}_r\mathbf{A}^{\varepsilon}_k$ contain the information about $\boldsymbol{\Phi}_r$ and $\boldsymbol{\Phi}^{\varepsilon}_r$, respectively.

2.3 Problems regarding the mass normalisation in the strain EMA

The displacement and strain mode shapes as a result of the strain EMA are not mass-normalised [3]. They are scaled by ϕ^{ε}_{jr} and ϕ_{kr}, respectively (see Eq. (5) and (6)).

In the classic EMA the mass normalisation is performed by taking into account the interrelation of the modal constants, which is described by the modal constant's consistency equations [1, 2]:

$$ {}_rA_{jk} = \phi_{jr}\,\phi_{kr} \tag{7}$$

$$ {}_rA_{jj} = (\phi_{jr})^2 \quad \text{or} \quad {}_rA_{kk} = (\phi_{kr})^2 \tag{8}$$

where ${}_rA_{jk}$ is the motion modal constant of the receptance between the response and the excitation structure points j and k, respectively. When the direct motion FRF is measured the ϕ_{jr} can be determined from the identified modal constant with Eq. (8) and used for a calculation of the mass-normalised displacement mode shapes $\boldsymbol{\Phi}_r$ [25].

In the strain EMA the modal constants are not interrelated like in the classic EMA (Section 2.1); therefore, the mass normalisation of the displacement and the strain mode shapes cannot be performed [3]. To calculate the $\boldsymbol{\Phi}_r$ and $\boldsymbol{\Phi}^{\boldsymbol{\varepsilon}}_r$, an artificial mass normalisation has to be performed in the strain EMA [3, 6, 7, 11].

2.4 Mass normalisation using the mass-change strategy in the OMA

In this research the mass normalisation in the strain EMA is performed with the mass-change strategy that is normally used for the mass normalisation of the displacement mode shapes in the OMA [15, 19]. It is based on the sensitivity of the modal parameters. The modal sensitivity of the eigenvalue $\Delta\,(\omega_{\mathrm{A},r})^2$ and the sensitivity of the eigenvector $\Delta\,\boldsymbol{\Phi}_{\mathrm{A},r}$ are written as [2]:

$$\Delta(\omega_{\mathrm{A},r})^2 \approx \sum_{i=1}^{N_p} \frac{\partial(\omega_{\mathrm{A},r})^2}{\partial p_i}\, p_i \tag{9}$$

and

$$\Delta\,\boldsymbol{\Phi}_{\mathrm{A},r} \approx \sum_{i=1}^{N_p} \frac{\partial \boldsymbol{\Phi}_{\mathrm{A},r}}{\partial p_i}\, p_i \tag{10}$$

where p_i is a generic parameter used to describe the dynamic model. $(\omega_{\mathrm{A},r})^2$ and $\boldsymbol{\Phi}_{\mathrm{A},r}$ are functions of p_i.

The process of the mass-change strategy for the OMA is shown in Fig. 1. First, the OMA is performed on an original structure to determine the natural frequencies ω_r, the unnormalised displacement mode shapes $\boldsymbol{\Psi}_r$ and the damping. This is followed by the structure modification by attaching the lumped masses, which leads to a change of the natural frequencies [15]. The strategy of the structure modification will be discussed later. Next, the OMA is performed again on the modified structure to determine the natural frequencies $\omega_{\mathrm{m},r}$ and the unnormalised displacement mode shapes $\boldsymbol{\Psi}_{\mathrm{m},r}$ of the modified structure. Finally, the OMA results of an original and a modified structure are used for the calculation of the scaling factors α_r, which are used for the calculation of $\boldsymbol{\Phi}_r$. The relation between $\boldsymbol{\Psi}_r$ and $\boldsymbol{\Phi}_r$ is expressed as [15, 18]:

$$\boldsymbol{\Phi}_r = \alpha_r\, \boldsymbol{\Psi}_r \tag{11}$$

Several approaches have been developed for the calculation of the scaling factors. Some of them are considered in this article. Parloo *et al.* [15] developed an approach that uses a first-order approximation for the sensitivity of the natural frequencies of lightly-damped structures. It is defined as:

$$\alpha_r = \sqrt{\frac{2(\omega_r - \omega_{\mathrm{m},r})}{\omega_r\, \boldsymbol{\Psi}_r^{\mathrm{T}}\, \Delta\mathbf{m}\, \boldsymbol{\Psi}_r}} \tag{12}$$

where $\Delta\mathbf{m}$ is the mass-change matrix. The application of this expression requires small frequency shifts and therefore small structure modifications. The authors suggest mass changes of around 5 %. Bricker and Anderson [16] presented an expression which is derived directly from equations of motion. It is defined as:

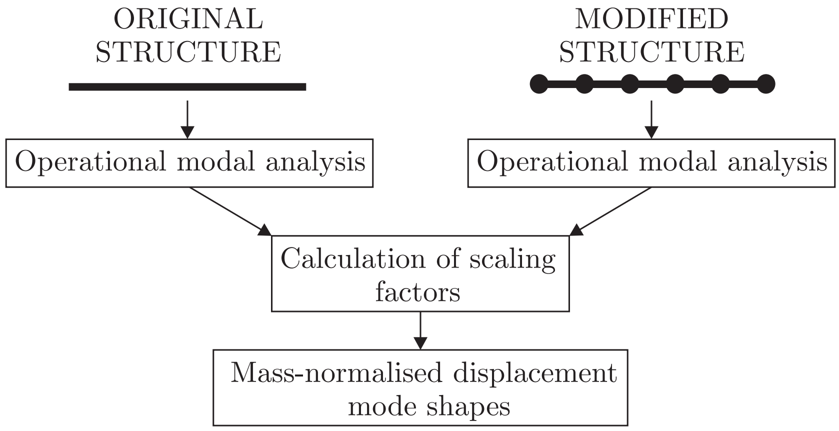

Fig. 1: The process of the mass-change strategy in the OMA [19]

$$\alpha_r = \sqrt{\frac{(\omega_r^2 - \omega_{\mathrm{m},r}^2)}{\omega_{\mathrm{m},r}^2 \, \mathbf{\Psi}_r^{\mathrm{T}} \, \mathbf{\Delta m} \, \mathbf{\Psi}_r}} \tag{13}$$

This expression should be used when the structure modification results only in the frequency shifts and the displacement mode shapes changes are small or zero. Aenlle *et al.* [18] presented an expression that considers the displacement mode shapes before and after the modification:

$$\alpha_r = \sqrt{\frac{(\omega_r^2 - \omega_{\mathrm{m},r}^2)}{\omega_{\mathrm{m},r}^2 \, \mathbf{\Psi}_r^{\mathrm{T}} \, \mathbf{\Delta m} \, \mathbf{\Psi}_{\mathrm{m},r}}} \tag{14}$$

They performed many simulations where the modification was performed with the randomly distributed masses. The results showed that Eq. (14) gives more accurate results than Eq. (13) when the displacement mode shapes are changed after the modification.

2.5 Mass normalisation with a mass-change strategy for the strain EMA

The mass-change strategy for the OMA was modified for use in the mass normalisation in the strain EMA. The procedure of the mass-change strategy for the strain EMA (Fig. 2) is similar to that in the OMA (Section 2.4).

First, the strain EMA is performed on an original structure to determine the information about displacement mode shapes ${}_r\mathbf{A}_j^{\varepsilon}$, the strain mode shapes ${}_r\mathbf{A}_k^{\varepsilon}$, the natural frequencies ω_r and the damping of the structure. The unnormalised displacement and strain mode shapes are identified from the jth row and the kth column of the strain FRF matrix, respectively (Section 2.2). Then the structure

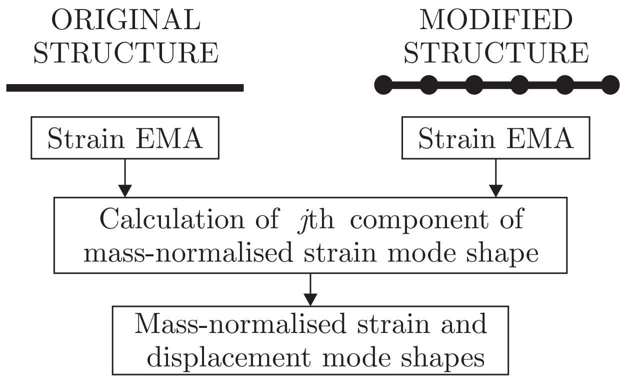

Fig. 2: The process of the mass-change strategy in the strain EMA

modification is performed in the same way as in the mass-change strategy for the OMA. Next, the strain EMA is performed on a modified structure to determine the information about the displacement mode shapes ${}_r\mathbf{A}^{\varepsilon}_{\mathrm{m},j}$ and the natural frequencies $\omega_{\mathrm{m},r}$ of the modified structure.

Finally, the calculation of the scaling factors for the mass normalisation in the strain EMA follows. Replacing $\mathbf{\Psi}_r$ in Eq. (11) with the identified displacement mode shape (unnormalised) ${}_r\mathbf{A}^{\varepsilon}_j$ leads to the relation:

$$\alpha_r = (\phi^{\varepsilon}_{jr})^{-1} \tag{15}$$

which shows, that the scaling factor for the rth mode is the jth inverse component of the mass-normalised strain mode shape $\mathbf{\Phi}^{\boldsymbol{\varepsilon}}_r$. The expressions for the calculation of the scaling factors using the mass-change strategy (Section 2.4) are modified for the calculation of $\phi^{\boldsymbol{\varepsilon}}_{jr}$. By considering the relation (15) the Eq. (12-14) can be rewritten as:

$$_{\mathrm{MC}}\phi^{\varepsilon}_{jr} = \sqrt{\frac{\omega_r\,({}_r\mathbf{A}^{\varepsilon}_j)^{\mathrm{T}}\,\Delta\mathbf{m}\,({}_r\mathbf{A}^{\varepsilon}_j)}{2\,(\omega_r-\omega_{\mathrm{m},r})}}, \tag{16}$$

$$_{\mathrm{MC}}\phi^{\varepsilon}_{jr} = \sqrt{\frac{\omega^2_{\mathrm{m},r}\,({}_r\mathbf{A}^{\varepsilon}_j)^{\mathrm{T}}\,\Delta\mathbf{m}\,({}_r\mathbf{A}^{\varepsilon}_j)}{(\omega^2_r-\omega^2_{\mathrm{m},r})}}, \tag{17}$$

and

$$_{\mathrm{MC}}\phi^{\varepsilon}_{jr} = \sqrt{\frac{\omega^2_{\mathrm{m},r}\,({}_r\mathbf{A}^{\varepsilon}_j)^{\mathrm{T}}\,\Delta\mathbf{m}\,({}_r\mathbf{A}^{\varepsilon}_{\mathrm{m},j})}{(\omega^2_r-\omega^2_{\mathrm{m},r})}} \tag{18}$$

where ${}_{\mathrm{MC}}\phi^{\varepsilon}_{jr}$ is the jth component of $\mathbf{\Phi}^{\varepsilon}_r$ that is estimated with the mass-change strategy for the strain EMA. Regarding the variability of the mass changes, the application possibilities of Eq. (16), Eq. (17) and Eq. (18) are the same as for Eq. (12), Eq. (13) and Eq. (14), respectively. ${}_{\mathrm{MC}}\phi^{\varepsilon}_{jr}$ is used for a determination of the mass-normalised displacement and strain mode shapes by using the following equations:

$$\mathbf{\Phi}_r = \pm \frac{{}_r\mathbf{A}^{\varepsilon}_j}{{}_{\mathrm{MC}}\phi^{\varepsilon}_{jr}} \tag{19}$$

$$\mathbf{\Phi}^{\varepsilon}_r = \pm \frac{{}_r\mathbf{A}^{\varepsilon}_k \, {}_{\mathrm{MC}}\phi^{\varepsilon}_{jr}}{{}_r A^{\varepsilon}_{jk}} \tag{20}$$

In general, the sign of $\mathbf{\Phi}_r$ can be positive or negative [1, 2]. To determine the $\mathbf{\Phi}^{\varepsilon}_r$ which are orientated corresponding to $\mathbf{\Phi}_r$ the sign in Eq. (20) has to be the same as in Eq. (19).

2.6 Accuracy analysis of the mass-change strategy for the strain EMA

The effects on the accuracy of the results of the mass-change strategy for OMA has been well researched [15, 16, 19, 20]. In [15, 16] the accuracy was researched especially regarding the quality of the modal parameter identification. The importance of the magnitude, the location and the number of attached masses was shown in [19] and experimentally investigated in [20]. In this section the effects on the accuracy of the proposed approach will be researched regarding the quality of the modal parameter identification and also the parameters of the structure modification.

2.6.1 The quality of modal parameter identification

The relative error as a result of the uncertainty in the identified natural frequencies is estimated by differentiating Eq. (17) with respect to the frequency ratio $\eta_\omega = \frac{\omega_r}{\omega_{\mathrm{m},r}}$ (see [19]):

$${}_{\mathrm{MC}}\varepsilon_{\phi^{\varepsilon}_{jr}} = \frac{\delta \, {}_{\mathrm{MC}}\phi^{\varepsilon}_{jr}}{{}_{\mathrm{MC}}\phi^{\varepsilon}_{jr}} = -\frac{\eta^2_\omega}{\eta^2_\omega - 1} \frac{\delta \, \eta_\omega}{\eta_\omega} = \frac{\eta^2_\omega}{\eta^2_\omega - 1} \left(\frac{\delta \, \omega_{\mathrm{m},r}}{\omega_{\mathrm{m},r}} - \frac{\delta \, \omega_r}{\omega_r} \right) \tag{21}$$

where ${}_{\mathrm{MC}}\varepsilon_{\phi^{\varepsilon}_{jr}}$ is the relative error of ${}_{\mathrm{MC}}\phi^{\varepsilon}_{jr}$, $\frac{\delta \, \eta_\omega}{\eta_\omega}$ is the relative error of the η_ω, $\frac{\delta \, \omega_r}{\omega_r}$ and $\frac{\delta \, \omega_{\mathrm{m},r}}{\omega_{\mathrm{m},r}}$ are the relative errors of the natural frequencies corresponding to the original and modified structure, respectively. Eq. (21) shows that the frequency ratio η_ω should be large in order to minimize the effects of the errors of the estimated natural frequencies.

The relative error ${}_{\mathrm{MC}}\varepsilon_{\phi^{\varepsilon}_{jr}}$ is also analyzed with respect to the relative error of the displacement mode shapes ${}_r\mathbf{A}^{\varepsilon}_j$ (a result of the strain EMA). It is estimated by the differentiation of Eq. (17) with respect to the component of the identified strain modal constant ${}_r A^{\varepsilon}_{ji}$ at the ith location of the attached mass (see [15]):

$$
{}_{\mathrm{MC}}\varepsilon_{\phi^{\varepsilon}_{jr}} = \sum_{i=1}^{N_\mathrm{m}} \left(\frac{({}_rA^{\varepsilon}_{ji})^2\, \Delta\, \mathrm{m}_i}{({}_r\mathbf{A}^{\varepsilon}_j)^\mathrm{T}\, \mathbf{\Delta m}\, ({}_r\mathbf{A}^{\varepsilon}_j)} \, \frac{\delta({}_rA^{\varepsilon}_{ji})}{({}_rA^{\varepsilon}_{ji})} \right) \tag{22}
$$

where N_m is the number of attached masses, $\frac{\delta({}_rA^{\varepsilon}_{ji})}{({}_rA^{\varepsilon}_{ji})}$ is the relative error in ${}_rA^{\varepsilon}_{ji}$. Eq. (22) shows that when the components of ${}_r\mathbf{A}^{\varepsilon}_j$ are subjected to a similar relative error ε, the relative error of ${}_{\mathrm{MR}}\phi^{\varepsilon}_{jr}$ will be approximately ε [15].

2.6.2 Strategy of adding the masses

The accuracy of the mass change-strategy for strain EMA also depends on the strategy for attaching the masses [19, 20]. One one hand, the mass change should be performed in a way that ensures the large frequency shifts in order to perform quality natural frequencies identification and minimize the effects of the uncertainties (see Eq. 21). To analyze the natural frequency changes the frequency ratio η^2_ω is derived from Eq. (17):

$$
\eta^2_\omega = 1 + \left(\frac{1}{{}_{\mathrm{MR}}\phi^{\varepsilon}_{jr}} \right)^2 {}_r\mathbf{A}^{\varepsilon\,\mathrm{T}}_j\, \mathbf{\Delta m}\, {}_r\mathbf{A}^{\varepsilon}_j. \tag{23}
$$

The expression shows that the natural frequency shifts are a maximum when $\mathbf{\Delta m}$ is maximized and when the masses are attached to the peaks and valleys of the considered mode [19].

On the other hand, the displacement mode shapes must not be changed after the modification (see [16, 19, 20]). In [19] it is shown that the displacement mode shape's changes are minimized, when the mass-change matrix $\mathbf{\Delta m}$ is relatively small and proportional to the mass matrix $\mathbf{m}$ of a dynamical system. In practice, it is important to ensure that the number of masses is equal or higher than the number of peaks and valleys of the considered mode shape [19]. The listed facts show the complexity of performing the optimal mass-change modification; therefore, the attaching of the masses must be carefully studied with respect to the number, the location and the magnitude of the attached masses.

3 Experimental validation

In order to validate the proposed approach the experimental tests on a beam and a plate structure were performed.

3.1 Experimental tests on a beam structure

In the first case the experimental tests were made on a steel, 1-m-long, free-free supported beam with a rectangular, 0.01×0.03 m cross-section (Fig. 3 and 4). The free-free boundary conditions were achieved by suspending the structure from thin ropes (not visible in Fig. 3). Only the bending modes in the plane xy were considered, which results in displacements in the y-direction and normal strains in the x-direction [26]. The experiment was performed as follows. First, the strain EMA was performed and then the mass-normalisation procedure with the mass-change strategy for the strain EMA followed. The obtained results were compared to the results of the finite-element method (FEM) and then used for a reconstruction of the measured accelerance.

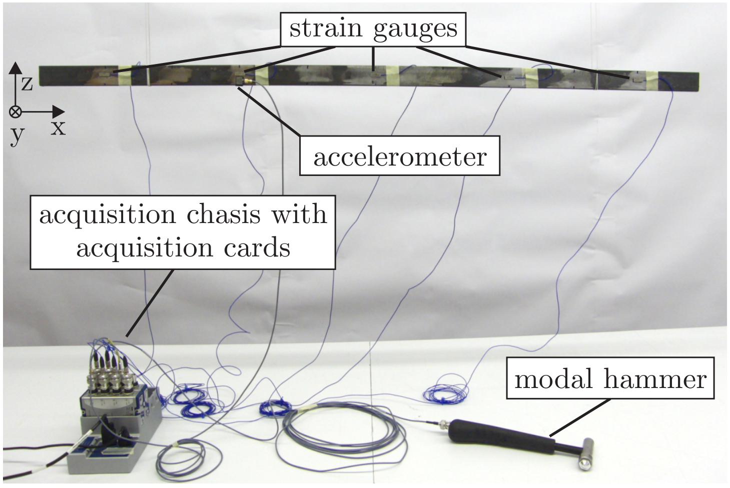

Fig. 3: The strain modal testing on the free-free supported beam

3.1.1 Strain EMA

During the strain modal testing the response was measured in the x-axis (Fig. 4) with calibrated strain gauges (PCB 740B02), while the structure was excited with a modal hammer (B&K Type 8206-002) in the y-axis. First, the responses were measured at structure point 4 (Fig. 4), while the structure was excited at the points 1-11 to determine the 4th row of the 11×11 sized strain FRF matrix (the number of the rows and columns is the same in this case). Then, the responses were measured at the points 2, 4, 6, 8, 10, while the structure was excited at the point 4 to determine the 4th column of the strain FRF matrix. With the five strain gauges that were attached to the structure, only the 2nd, 4th, 6th, 8th and 10th elements of the 4th column were measured.

The tested structures are lightly damped; therefore, the modal parameter identification was performed with the Ewins-Gleeson identification method [25], which was developed for such structures, assuming the hysteretic damping model. For such systems the mass-normalised displacement mode shapes are taken to be real (with phase angles of 0 or 180 degrees) [2]; therefore, they match the calculated (numerical) ones. As discussed in Section 2.2, the identified strain modal constants contain only the relative information about the mass-normalised displacement and the strain mode shapes. Fig. 5 shows the difference

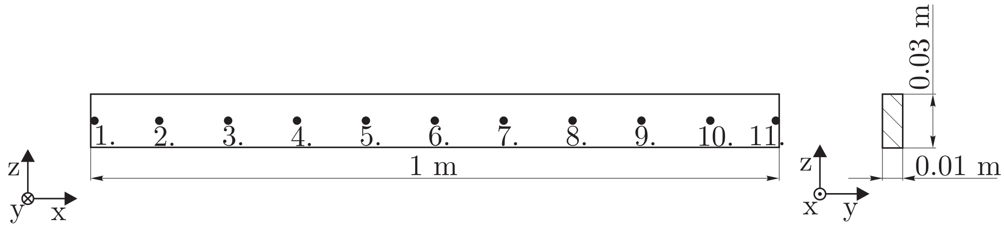

Fig. 4: The tested beam

between the mode shapes that were identified with the strain EMA and the calculated ones by FEM (mass-normalised). Fig. 5 (a,c,e,g,i) and Fig. 5 (b,d,f,h,j) show the first five displacement and strain mode shapes, respectively. The figure shows that the experimentally determined mode shapes are not in agreement with the calculated ones. The discrepancies are the result of the incorrect scaling. Therefore, the experimentally determined mode shapes match the calculated ones only in the mode shape nodes (*e.g.*, the structure point 6 at the 2nd displacement and strain mode shapes-Fig. 5 (c) and Fig. 5 (d)).

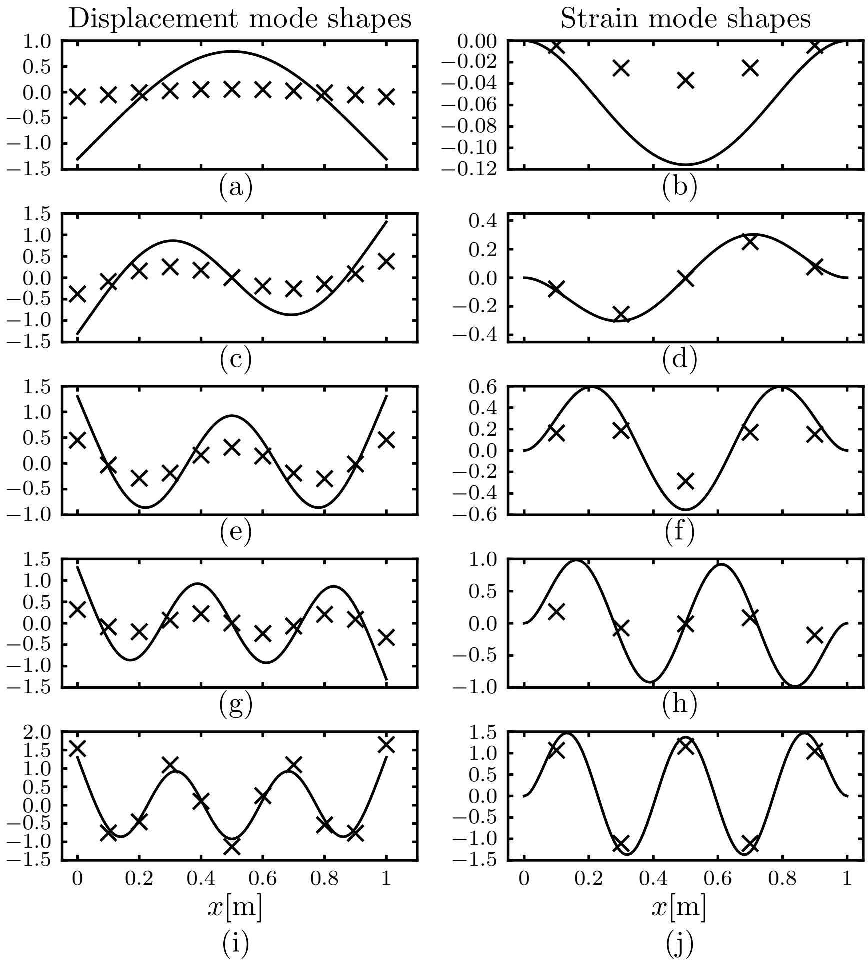

Fig. 5: The first five displacement (a,c,e,g,i) and strain (b,d,f,h,j) mode shapes: determined with the strain EMA (unnormalised) “×”, calculated using FEM (mass normalised) “—”

3.1.2 Mass normalisation with the mass-change strategy for the strain EMA

The displacement and strain mode shapes were mass normalised using the proposed mass-change strategy for the strain EMA. The procedure is described in Section 2.5. The strain EMA for the original structure follows the structure modification by attaching magnets to the structure points 1-11 (Fig. 4). Each of the magnets weighted 11.6 g, and the total mass of the magnets was approximately 5.4 % of the original structure weight. After the structure modification the strain EMA was performed for the modified structure once again. The natural frequencies of the modified beam were decreased by the added masses. The change is evident from Table 1, where f_r and $f_{\mathrm{m},r}$ are the natural frequencies of the original and modified structures, respectively, and δ_r is the relative change between the natural frequencies of the modified and original structures. As is clear from Section 2.2 the displacement mode shapes that are determined using the strain EMA are scaled by the jth component of the strain mode shape ϕ^{ε}_{jr}. To calculate ϕ^{ε}_{jr} one of the Eq. (16)-(18), which are presented in Section 2.5, can be used. In order to choose the appropriate approach a comparison of the displacement mode shapes before and after the structure modification was performed using the modal assurance criterion (MAC) [27]. The results of the MAC analysis (Fig. 6) show that the displacement mode shapes were not significantly changed by the structure modification; therefore, Eq. (17) was used. ${}_{\mathrm{MC}}\phi^{\varepsilon}_{4r}$ were calculated for all the modes and used to determine the mass-normalised displacement and the strain mode shapes $\mathbf{\Phi}_r$ and $\mathbf{\Phi}^{\boldsymbol{\varepsilon}}_r$ with Eq. (19) and (20). The $\mathbf{\Phi}_r$ and $\mathbf{\Phi}^{\boldsymbol{\varepsilon}}_r$ that were determined with the proposed approach are plotted together with the calculated ones using the FEM in Fig. 7. Fig. 7 (a,c,e,g,i) and Fig. 7 (b,d,f,h,j) show the first five displacement and strain mode shapes, respectively. The Figure shows that the experimental results match the calculated ones well.

Table 1: The natural frequencies of the original and the modified beams

r	f_r[Hz]	$f_{\mathrm{m},r}$[Hz]	δ_r
1	52.85	51.05	-3.41 %
2	145.45	140.45	-3.44 %
3	285.0	274.7	-3.61 %
4	471.1	454.2	-3.59 %
5	701.25	675.05	-3.74 %

The modal parameters that were determined with the proposed approach were used to reconstruct the direct accelerance at point 4, denoted as H^A_{44}. The reconstruction was also performed with the modal parameters that were identified from the measured accelerance H^A_{44}. The response was measured with the accelerometer B&K 4507B004 (Fig. 3). In Fig. 8 both reconstructed FRFs are shown together with the measured one. The reconstructed accelerances have approximately the same amplitudes and describe well the resonance peaks. The

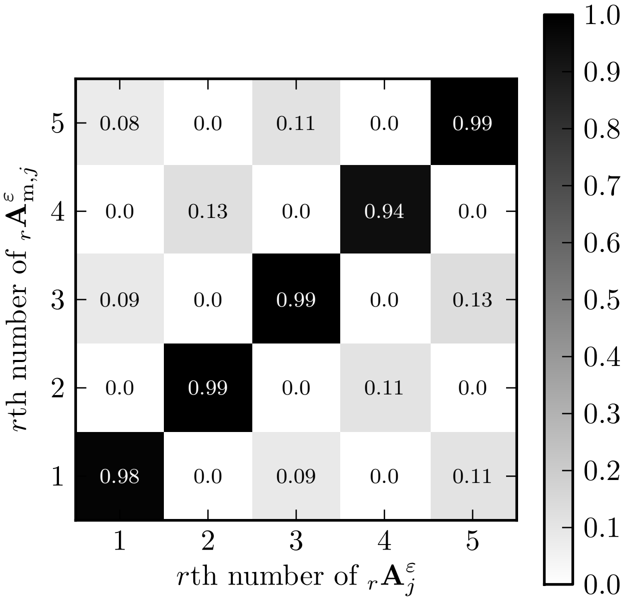

Fig. 6: The correlation between the displacement mode shapes of the original and the modified beams

discrepancy out of the resonance is a consequence of the residual modes that are not taken into account. Furthermore, the effects of the residual modes were estimated from the measured H^A_{44} using the extended Ewins-Gleeson identification method [25]. When the residues were taken into account both the reconstructed accelerances match the measured one better (Fig. 9).

The comparison with the results of the FEM and the accelerance reconstruction show the validity of the proposed approach for beam structures.

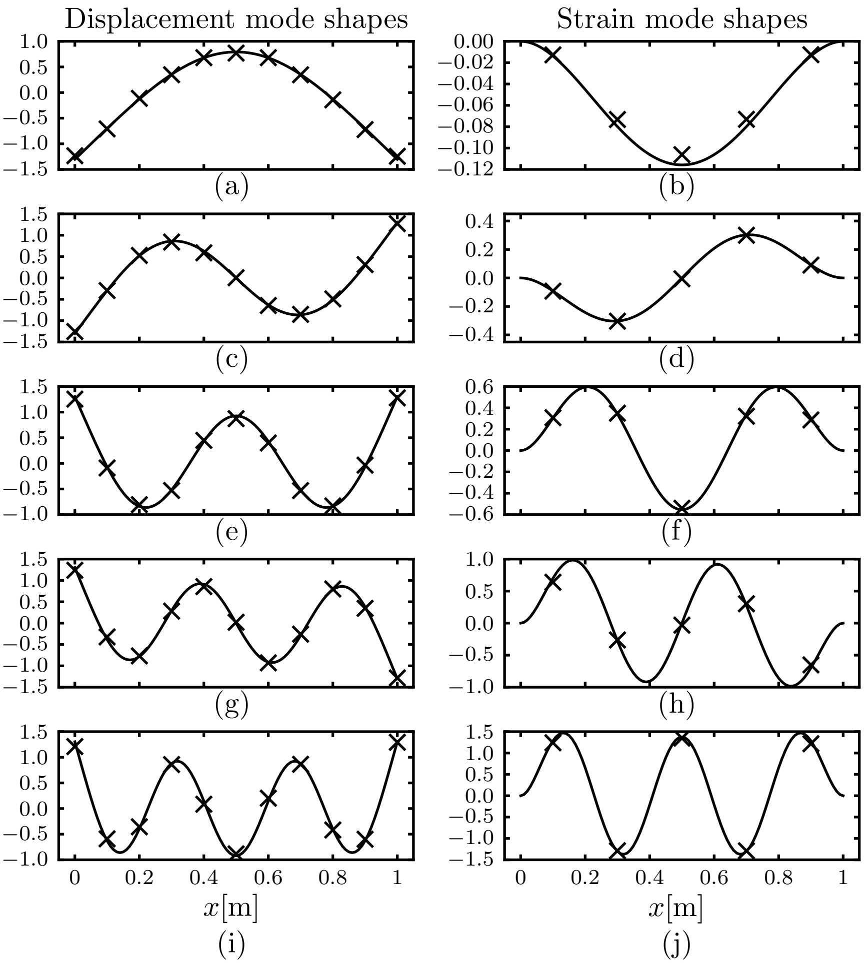

Fig. 7: The first five mass-normalised displacement (a,c,e,g,i) and strain (b,d,f,h,j) mode shapes; determined with the proposed approach "×", calculated using FEM "—"

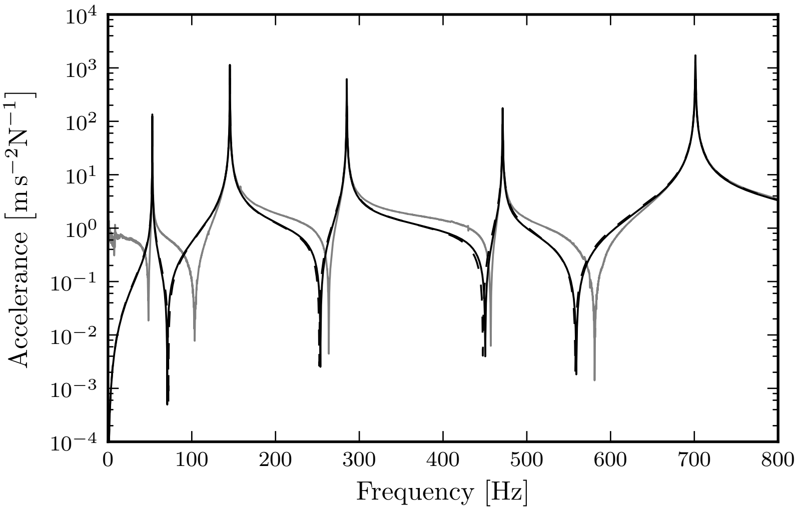

Fig. 8: The direct accelerance; measured (grey "—"), reconstructed from the measured accelerance (black "- - -") and from the proposed approach (black "—")

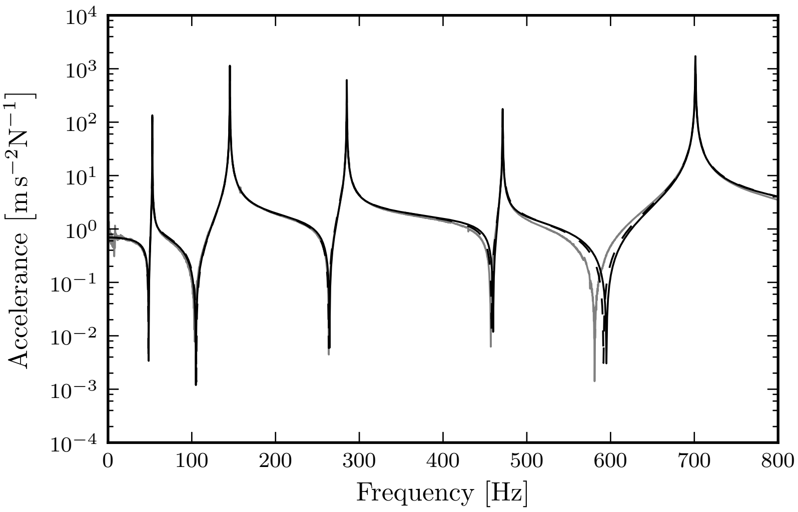

Fig. 9: The direct accelerance; measured (grey "—"), reconstructed (considering the residues) from the measured accelerance (black "- - -") and from the proposed approach (black "—")

3.2 Experimental testing on a plate structure

The second experimental case was performed on a steel, 0.4× 0.32× 0.003 m sized, free-free supported plate (Fig. 10).

We considered the first five modes, which vibrate out of plane xy and result in the normal and shear strains (stresses) [28]. The application of the proposed approach (Section 2.5) was shown by determining of the mass-normalised displacement mode shapes and the normal components of the mass-normalised strain mode shapes in the x-direction ($\mathbf{\Phi}_r^{\varepsilon_{xx}}$) and the y-direction ($\mathbf{\Phi}_r^{\varepsilon_{yy}}$).

The strain modal testing was performed with the same equipment as in the case of the beam (Section 3.1). To obtain the information about the displacement mode shapes the plate was excited with the modal hammer at the points 1-30 (Fig. 10) and the response was measured at the point 31. The information about the strain mode shapes was obtained by exciting the structure at the point 26 and measuring the normal x-components of the strains at the points 6, 11, 16, 21, 31 and the normal y-components at the points 2-4. The modal identification was performed in a similar way as in the case of the beam. Followed the mass normalisation by the proposed approach. In order to ensure that the mass change will not affect the displacement mode shapes, the magnets were attached as follows. At the points (7-9, 12-14, 17-19, 22-24), (2-4, 6, 10, 11, 15, 16, 20, 21, 25, 27-29) and (1, 5, 26, 30) the 11.6 g, 5.1 g and 3.6 g magnets were attached to the structure, respectively. The total mass of the magnets was approximately 6.6 % of the original structure's weight. The natural frequencies before and after the modification, which are denoted as f_r and $f_{\mathrm{m},r}$, respectively, are listed in Table 2. The relative frequency shifts are denoted as δ_r. The modification did not affect the displacement mode shapes. This was proved by the MAC comparison of ${}_r\mathbf{A}_j^{\varepsilon}$ and ${}_r\mathbf{A}_{\mathrm{m},j}^{\varepsilon}$, where the lower diagonal element of the MAC matrix was approximately 0.96. We used Eq. (17) for the calculation of ${}_{\mathrm{MC}}\phi_{31r}^{\varepsilon}$, which were then used for the mass-normalisation. The results of the testing were the components of $\mathbf{\Phi}_r$ at the points (1-30) and additionally, the components of $\mathbf{\Phi}_r^{\varepsilon_{xx}}$ and $\mathbf{\Phi}_r^{\varepsilon_{yy}}$ at the points (6, 11, 16, 21, 31) and (2-4), respectively.

Table 2: The natural frequencies of the original and the modified plates

r	f_r[Hz]	$f_{\mathrm{m},r}$[Hz]	δ_r
1	80.1	77.4	-3.4 %
2	98.2	94.6	-3.7 %
3	167.1	160.1	-4.2 %
4	191.8	184.8	-3.6 %
5	224.2	215.1	-4.1 %

The experimental results were compared to the results of the FEM. First, we compared the experimentally determined $\mathbf{\Phi}_r$ to the calculated ones. The relative comparison was performed by MAC analysis, where the lower diagonal element of the MAC matrix was approximately 0.96. The graphical comparison

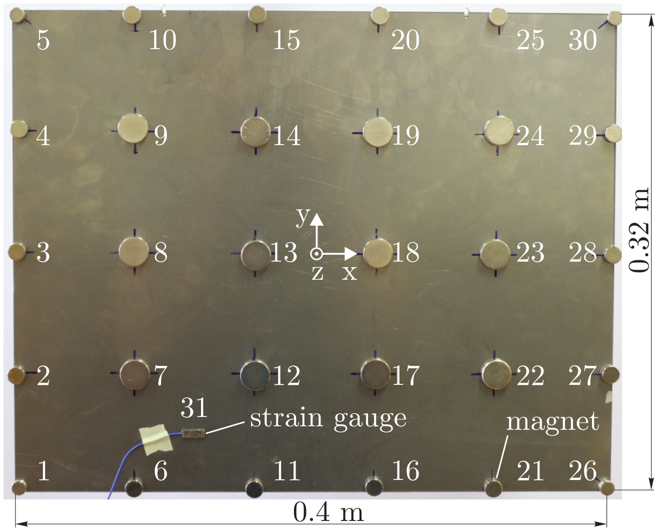

Fig. 10: The experimental testing on the free-free supported plate

was performed by plotting the experimentally determined $\mathbf{\Phi}_r$ and the calculated ones together in Fig. 11. Fig. 11 (a,c,e,g,i) show $\mathbf{\Phi}_r$ for the structure points 1-30. The detailed plots are shown in Fig. 11 (b,d,f,h,j), where only the components of $\mathbf{\Phi}_r$ at the location $y = -0.08$ m are plotted. Then, the experimentally determined components of $\mathbf{\Phi}_r^{\varepsilon}$ were compared to the calculated ones by FEM in Fig. 12. Fig. 12 (a,c,e,g,i) show the $\mathbf{\Phi}_r^{\varepsilon xx}$ at the location $y = -0.16$ m. Fig. 12 (b,d,f,h,j) show $\mathbf{\Phi}_r^{\varepsilon yy}$ at the location $x = -0.2$ m. The experimentally determined components of $\mathbf{\Phi}_r$ and $\mathbf{\Phi}_r^{\varepsilon}$ are in good agreement with the calculated ones, although there are some discrepancies. These come from several error sources: the measuring errors, the local stiffness changes due to the strain gauges that are attached to the relatively thin sheet metal and the deviations of the stain-gauge attachment regarding the position and the angle.

The results of the proposed approach were used for the reconstruction of the direct accelerance at point 26 (similarly as in the Fig. 9). It was also reconstructed from the modal parameters that were identified from the measured accelerance. The reconstructed accelerances are plotted together with the measured one in Fig. 13. Both reconstructed accelerances are in good agreement with the measured one. The results of the experiment show the validity of the proposed approach for the plate structure.

4 Conclusion

In this research we considered the problems relating to mass normalisation (scaling) of displacement and strain mode shapes in the strain EMA. The mass-

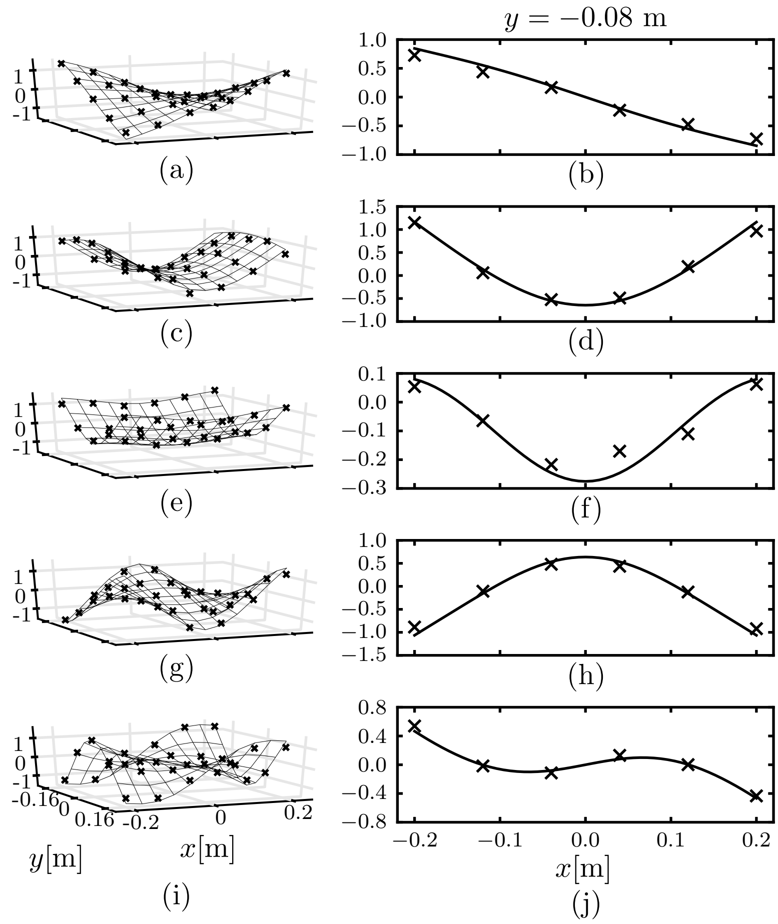

Fig. 11: The first five mass-normalised displacement mode shapes ((a,c,e,g,i)-all the measuring points, (b,d,f,h,j)-points at y=-0.08 m) ; calculated (—) and experimentally determined (×)

normalised displacement and strain mode shapes, are in the strain EMA, usually experimentally obtained in combination with the classic EMA, where a direct motion FRF has to be measured. A new approach to mass normalisation in the strain EMA is presented, which requires only the strain FRF measurements. The approach enables a mass-normalisation procedure in the strain EMA even when a motion sensor cannot be used. The proposed approach is based on the recently introduced mass-change strategy for mass normalisation in the OMA. In this research the mass-change strategy was modified for use with the strain EMA. The mass-normalised displacement and strain mode shapes were obtained by a combination of the strain EMA and the proposed approach. The accuracy

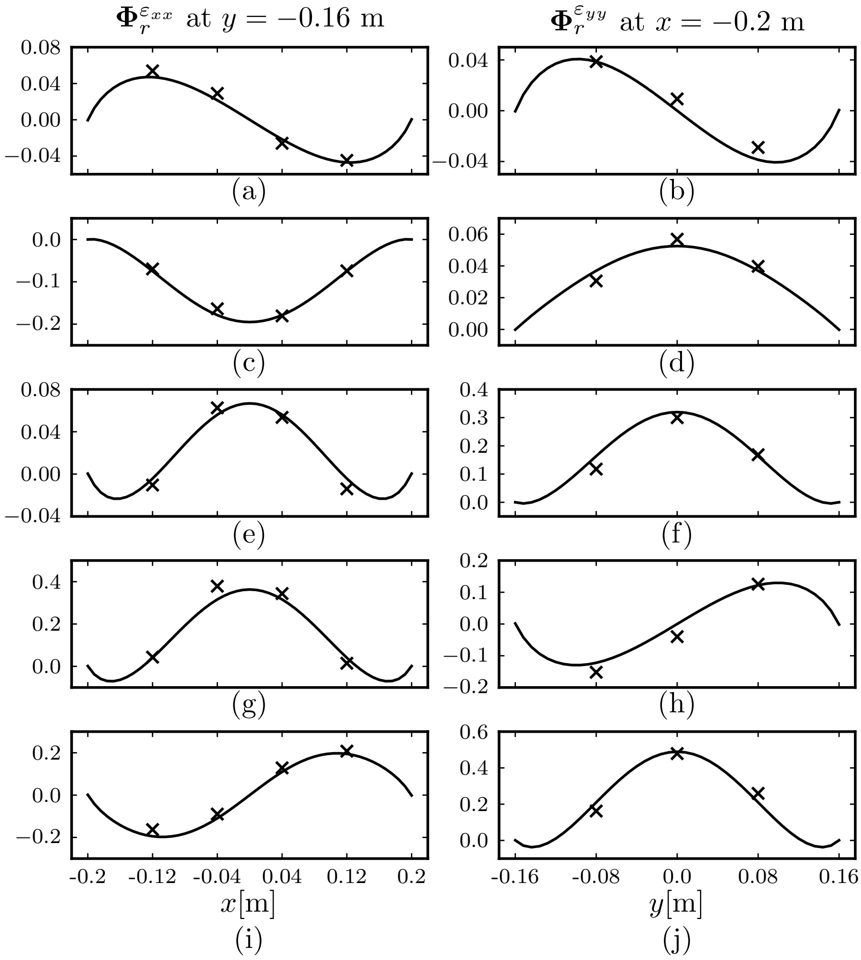

Fig. 12: Components of the first five mass-normalised strain mode shapes ((a,c,e,g,i)-$\mathbf{\Phi}_r^{\varepsilon_{xx}}$, (b,d,f,h,j)-$\mathbf{\Phi}_r^{\varepsilon_{yy}}$); calculated (—) and experimentally determined ($\times$)

of the proposed approach was researched with respect to the quality of the modal parameter identification and the number, the magnitude and the location of the attached masses.

The approach was experimentally validated by tests on free-free supported beam and plate structures. We obtained the mass-normalised displacement and strain mode shapes of the structures, which match the shapes that were calculated with the FEM. The results of the proposed approach were also used for the reconstruction of the measured direct accelerances. The reconstructed accelerances are in good agreement with the reconstructed ones from the results of the

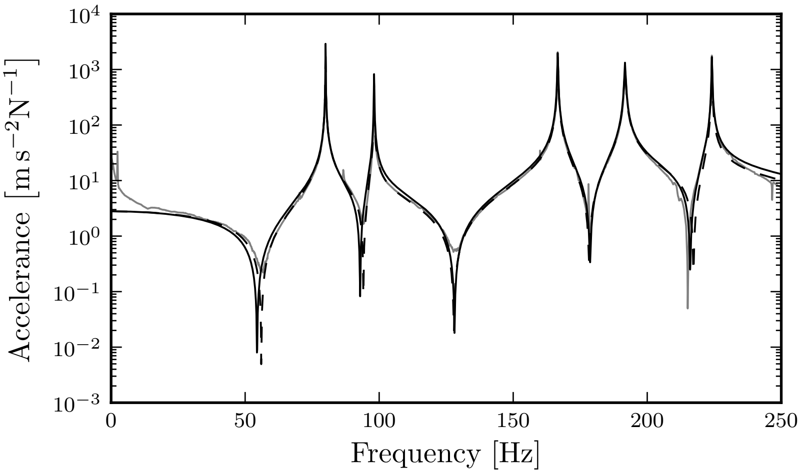

Fig. 13: The direct accelerance; measured (grey "—"), reconstructed from the measured accelerance (black "- - -") and from the proposed approach (black "— ")

classic EMA and also with the measured ones. The results of the experimental tests show the validity of the proposed approach.

Acknowledgement

The operation was partially Financed by the European Union, European Social Fund.

References

[1] D. Ewins, Modal testing: Theory and practice, Mechanical engineering research studies: Engineering dynamics series, Research Studies Press, 1984.

[2] N. Maia, J. Silva, Theoretical and Experimental Modal Analysis, Mechanical Engineering Research Studies: Engineering Dynamics Series, John Wiley & Sons, Limited, 1997.

[3] O. Bernasconi, D. J. Ewins, Modal strain/stress fields, The International Journal of Analytical and Experimental modal analysis 4 (2) (1989) 68–76.

[4] Z. Fu, J. He, Modal Analysis, Elsevier Science, 2001.

[5] W. Heylen, S. Lammers, P. Sas, Modal Analysis Theory and Testing, Haverlee: Katholieke Universiteit Leuven, 2007.

[6] O. Bernasconi, D. J. Ewins, Application of strain modal testing to real structures, in: Proceedings of the 7th International Modal Analysis Conference (IMAC-VII), 1989, pp. 1453–1464.

[7] D. Li, H. Zhuge, B. Wang, The principle and techniques of experimental strain modal analysis, in: Proceedings of the 7th International Modal Analysis Conference (IMAC-VII), 1989, pp. 1285–1289.

[8] B. Hillary, D. J. Ewins, The use of strain gauges in force determination and frequency response function, in: Proceedings of the 2nd International Modal Analysis Conference (IMAC-II), London, United Kingdom, 1984, pp. 627–634.

[9] J. W. Young, J. Joanides, Development of test-derived strain modal models for structural fatigue certification of the space shuttle orbiter, in: Proceedings of the 1st International Modal Analysis Conference (IMAC-I), 1982, pp. 479–487.

[10] J. M. Kamrower, P. M. P., Verification of modal testing and analysis techniques for prediction of dynamic strain in impact loaded structures, in: Proceedings of the 2nd International Modal Analysis Conference (IMAC-II), 1984, pp. 620–626.

[11] L. Yam, T. Leung, D. Li, K. Xue, Theoretical and experimental study of modal strain analysis, Journal of Sound and Vibration 191 (2) (1996) 251 – 260.

[12] D. C. Betz, L. Staudigel, M. N. Trutzel, M. Kehlenbach, Structural monitoring using fiber-optic bragg grating sensors, Structural Health Monitoring 2 (2) (2003) 145–152.

[13] J. J. Dosch, Air bearing shaker for precision calibration of accelerometers, in: Proceedings of the 24th International Modal Analysis Conference (IMAC-XXIV), St Louis , Missouri, U.S.A., 2006.

[14] L. Zhang, R. Brincker, P. Andersen, An overview of operational modal analysis: Major development and issues, in: Proceedings of the 22th International Modal Analysis Conference (IMAC-XXII), 2004, pp. 179–190.

[15] E. Parloo, P. Verboven, P. Guillaume, M. Van Overmeire, Sensitivity-based operational mode shape normalisation, Mechanical Systems and Signal Processing 16 (5) (2002) 757–767.

[16] R. Brincker, A. Anderson, A way of getting scaled modal shapes in output only modal analysis, in: Proceedings of the 21st International Modal Analysis Conference (IMAC-XXI), USA, 2003, pp. 141–145.

[17] R. Brincker, J. Rodrigues, P. Andersen, Scaling the mode shapes of a building model by mass changes, in: Proceedings of the 22nd Internationam Modal Analysis Conference (IMAC-XXII), Detroid, Michigam, USA, 2004, pp. 119–126.

[18] M. Lopez Aenlle, R. Brincker, A. Fernandez Canteli, Some methods to determine scaled mode shapes in natural input modal analysis, in: Proceedings of the 23th International Modal Analysis Conference (IMAC-XXIII), Orlando, Florida, U.S.A., 2005.

[19] M. Lopez-Aenlle, P. Fernandez, R. Brincker, A. Fernandez-Canteli, Erratum to scaling-factor estimation using an optimized mass-change strategy, Mechanical Systems and Signal Processing 24 (8) (2010) 3061–3074.

[20] G. Coppotelli, On the estimate of the FRFs from operational data, Mechanical Systems and Signal Processing 23 (2) (2009) 288 – 299.

[21] M. Khatibi, M. Ashory, A. Malekjafarian, R. Brincker, Mass stiffness change method for scaling of operational mode shapes, Mechanical Systems and Signal Processing 26 (0) (2012) 34 – 59.

[22] O. Zienkiewicz, R. Taylor, The Finite Element Method Set, Elsevier Science, 2005.

[23] L. Y. Yam, D. B. Li, T. P. Leung, K. Z. Xue, Experimental study on modal strain analysis of rectangular thin plates with small holes, in: Proceedings of the 12th International Modal Analysis Conference (IMAC-XII), 1994, pp. 1415–8.

[24] J. Slavič, I. Simonovski, M. Boltežar, Damping identification using a continuous wavelet transform: application to real data, Journal of Sound and Vibration 262 (2) (2003) 291–307.

[25] D. Ewins, P. Gleeson, A method for modal identification of lightly damped structures, Journal of Sound and Vibration 84 (1) (1982) 57 – 79.

[26] D. Hutton, Fundamentals of Finite Element Analysis, Engineering Series, McGraw-Hill Professional Publishing, 2003.

[27] A. R.J., A correlation coefficient for modal vector analysis, in: Proceedings of the 1st International Modal Analysis Conference (IMAC-I), Orlando, Florida, U.S.A., 1982, pp. 110–116.

[28] A. Leissa, Vibration of plates, NASA SP, Scientific and Technical Information Division, National Aeronautics and Space Administration, 1969.